Performance Evaluation of Leader–Follower-Based Mobile Molecular Communication Networks for Target Detection Applications

Tadashi Nakano, *Member, IEEE*, Yutaka Okaie, Shouhei Kobayashi, Takako Koujin, Chen-Hao Chan, Yu-Hsiang Hsu, *Member, IEEE*, Takuya Obuchi, Takahiro Hara, *Senior Member, IEEE*, Yasushi Hiraoka, and Tokuko Haraguchi

***Abstract*— This paper proposes a leader–follower-based model of mobile molecular communication networks for target detection applications. The proposed model divides the application functionalities of molecular communication networks into two types of mobile bio-nanomachine: leader and follower bio-nanomachines. Leader bio-nanomachines distribute in the environment to detect a target and create an attractant gradient around the target. Follower bio-nanomachines move according to the attractant gradient established by leader bio-nanomachines; they approach the target and perform necessary functionalities, such as releasing drug molecules. This paper develops mathematical expressions for the proposed model, describes wet laboratory experiments designed to estimate model parameters, and performs biologically realistic computer simulation experiments to evaluate the performance of the proposed model. The main contributions of this paper are to demonstrate the functional division of molecular communication networks, which will facilitate the design and development of molecular communication networks. Furthermore, insight into the application-level performance of molecular communication networks will be provided based on the proposed model.**

***Index Terms*— Mobile molecular communication network, bio-nanomachine, leader-follower model, collective behavior, target detection, targeted drug delivery, haptotaxis.**

I. Introduction

MOLECULAR communication networks, namely, collections of bio-nanomachines that communicate through molecular communication, are expected in the future to perform complex functionalities within biological systems [1]–[5]. Example applications of such networks are diverse and include transporting drug molecules to target locations (e.g., disease sites) [6], [7], releasing drug molecules at target locations [8]–[11], and tracking the locations of mobile targets inside the human body [12]–[14].

In designing molecular communication networks for specific applications, the central question is how required functionalities are distributed over a collection of bio-nanomachines. One approach adopted previously is based on the *all-in-one* model, where fully functional and identical bio-nanomachines are used to achieve application-dependent goals [6], [12], [15], [16]. This model, however, may not apply to cases where a single bio-nanomachine needs to implement a number of functionalities such as sensing the environmental conditions, producing directional motion, synthesizing molecules, and storing molecules. In such cases, an alternative approach is to divide a full set of functionalities into subsets of functionalities, prepare functionally different bio-nanomachines that each implement one of these subsets, and allow those bio-nanomachines to communicate, in order to achieve application-dependent goals.

In this paper, we propose the leader-follower-based model (LF model) of mobile molecular communication networks based on the principle of functional division and apply the model to targeted drug delivery.[1] The LF model divides key functionalities of mobile molecular communication networks into leader and follower bio-nanomachines. Leader bio-nanomachines distribute in the environment to detect a target. Upon detecting a target, leader bio-nanomachines release an attractant molecule, creating an attractant gradient around the target. Follower bio-nanomachines move in response to the attractant gradient made by leader bio-nanomachines; they approach the target and perform required functionalities such as releasing drug molecules.

In the area of drug delivery, functional division has been demonstrated in [18], in which two types of nanoparticle (signaling and receiving modules) cooperate to deliver drug molecules. The signaling modules are first targeted to tumors to activate tumor-specific endogenous biological pathways. The receiving modules carrying drug molecules in the

Manuscript received June 30, 2016; revised September 14, 2016; accepted November 1, 2016. Date of publication November 11, 2016; date of current version February 14, 2017. This work was supported by JSPS KAKENHI Grant Number JP25240011 and by the Osaka University Humanware Innovation Leading Graduate School Program. The associate editor coordinating the review of this paper and approving it for publication was M. Pierobon.

T. Nakano, Y. Okaie, and Y. Hiraoka are with the Graduate School of Frontier Biosciences, Osaka University, Osaka 565-0871, Japan (e-mail: tadasi.nakano@fbs.osaka-u.ac.jp; yokaie@fbs.osaka-u.ac.jp; hiraoka@fbs.osaka-u.ac.jp).

S. Kobayashi, T. Koujin, and T. Haraguchi are with the National Institute of Information and Communications Technology, Kobe 651-2492, Japan (e-mail: skobayashi@nict.go.jp; koujin@nict.go.jp; tokuko@nict.go.jp).

C.-H. Chan and Y.-H. Hsu are with the Institute of Applied Mechanics, National Taiwan University, Taipei 106, Taiwan (e-mail: cchao@ntumems.net; yhhsu@iam.ntu.edu.tw).

T. Obuchi and T. Hara are with the Graduate School of Information Science and Technology, Osaka University, Osaka 565-0871, Japan (e-mail: obuchi.takuya@ist.osaka-u.ac.jp; hara@ist.osaka-u.ac.jp).

Color versions of one or more of the figures in this paper are available online at http://ieeexplore.ieee.org.

Digital Object Identifier 10.1109/TCOMM.2016.2628037

[1] The early version of the paper appears in [17].

circulation respond to the activated tumor-specific biological pathways and efficiently accumulate at the tumor location. Functional division has also been discussed in [11] where liposome-based drug delivery is developed and analyzed. In [11], a transmitter releases prodrugs and a receiver contains an enzyme that can activate those prodrugs. The work described in this paper is in line with these efforts while focusing on autonomous and self-organized mobile molecular communication networks to control the spatial distribution of mobile bio-nanomachines.

The main contributions of this paper are as follows:

- A new model for mobile molecular communication networks is developd and presented. The proposed model facilitates design improvements and the further development of bio-nanomachines by reducing the number of functionalities that need to be implemented on individual bio-nanomachines.
- Mathematical techniques and wet laboratory experimental results are combined to develop a biologically realistic model of bio-nanomachines. This allows one to perform in silico experiments to understand and predict the behavior of mobile molecular communication networks.
- Simulation experiments investigate the application-level performance of mobile molecular communication networks based on the LF model and the all-in-one model for a range of settings. Simulation results provide an insight into the detailed behavior of mobile molecular communication networks, including optimal numbers of leader and follower bio-nanomachines and the relationship between a model parameter and the application-level performance of mobile molecular communication networks.

The reminder of this paper is organized as follows. Section II gives an overview of the LF model used in this paper. Section III develops mathematical expressions for the LF model, and Section IV describes techniques to estimate model parameters from wet laboratory experimental results. Based on the mathematical model and estimated parameters, Section V shows outcomes from computer simulation experiments and investigates the application-level performance of mobile molecular communication networks developed based on the LF model and the all-in-one model. Finally, Section VI summarizes this work and provides conclusions.

II. Overview

This paper considers drug delivery [19], [20] as an application of mobile molecular communication networks. The goal of drug delivery is to develop drug carriers that can be targeted to disease sites in the human body and can release drug molecules only at these disease sites, thus reducing the risk of side effects at non-disease sites. A key functionality of drug delivery is therefore the spatial control of drug carriers. This is for instance possible with liposome-based drug carriers whose surfaces express specific ligands that can bind to disease sites (e.g., cell-surface receptors of tumor cells). Another key functionality is the temporal control of drug release, which involves releasing drug molecules only when needed. This is possible with drug carriers that can release drug molecules in response to chemical and physical properties specific to disease sites (e.g., pH, temperature or concentration of glucose) or to externally applied stimuli (e.g., ultrasound, light or magnetic fields).

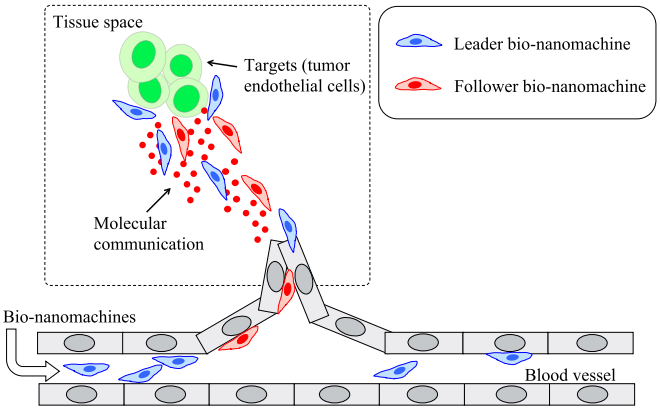

Fig. 1. Leader-follower-based mobile molecular communication network proposed in this paper.

As will be detailed in this section, this paper focuses on the spatial control of mobile bio-nanomachines for drug delivery. The specific application scenario considered in this paper consists of (1) distributing mobile bio-nanomachines in the environment, (2) identifying the location of a target in the environment, and (3) directing bio-nanomachines to the target location where they perform collective actions such as releasing drug molecules.

In the following, we first describe key components of mobile molecular communication networks for the application scenario described above; we also describe our assumptions with relevant background knowledge in biology (Section II-A). We will then describe a leader-follower based model of mobile molecular communication networks to control the spatial distribution of mobile bio-nanomachines (Section II-B).

A. Key Components

The **monitoring environment** we consider in this paper is aqueous and it contains molecules and energy sources for bio-nanomachines to perform necessary functionalities. The environment may also contain noise sources such as thermal noise and other molecules (noise molecules) that may interfere with bio-nanomachine functionalities. An example of the monitoring environment in a biological context could be the tissue space surrounding blood vessels (Fig. 1).

Targets are biochemical objects that appear in the monitoring environment. Targets are assumed to be chemically identifiable. For instance, targets may express specific proteins on their surface, and bio-nanomachines may physically interact with target surface receptors to identify the targets. Targets may also secrete diffusive marker molecules which bio-nanomachines are designed to detect. Targets may also migrate in the environment. An example of targets is tumor endothelial cells (Fig. 1). In the human body, morphological abnormalities in blood vessels are often observed where tumor endothelial cells are present [21] (see the abnormal sprout in Fig. 1). Such morphological abnormalities in blood vessels or other anomalies (e.g., inflammation in blood vessels) may be targets to which bio-nanomachines are delivered.

A **bio-nanomachine** is defined on the basis of three criteria: material, size and functionality [22]. A bio-nanomachine is composed of biomaterials (e.g., proteins, nucleic acids, lipids, biological cells) with or without non-biomaterials (e.g., magnetic particles and gold nanorods) [23]. The size of a bio-nanomachine ranges from the size of a macromolecule to that of a biological cell (i.e., dimensions of 1 – 100 μm). A bio-nanomachine implements a set of simple functionalities to manipulate molecules, such as detecting, modifying and releasing molecules. A bio-nanomachine may display mobility to produce directional motion in the monitoring environment; such bio-nanomachines are called *mobile* bio-nanomachines. In biology, many cell types produce directional motion through a process called chemotaxis [24], [25]. For molecular communication, mobile bio-nanomachines are used to deliver messages [26]. They are also assumed in the design of various networking mechanisms such as routing [27]–[29]. The specific bio-nanomachines assumed in this paper are genetically-modified endothelial cells (Fig. 1). In the human body, endothelial cells form blood vessels and are capable of migrating to almost every region of the body [30]. They also circulate in blood vessels to help in their regeneration and repair.

Via a process of molecular communication, bio-nanomachines form a **molecular communication network**. Two types of molecular communication exist: diffusion-based and non-diffusion-based. In diffusion-based molecular communication, bio-nanomachines communicate by propagating diffusive molecules in the environment. This type of molecular communication is found in natural and engineered molecular communication networks such as cooperative bacterial networks where bacteria secrete and diffuse N-acyl homoserine lactones (AHL) for quorum sensing [31] and for engineering applications [32], [33]. On the other hand, in non-diffusion-based molecular communication, bio-nanomachines communicate by using adhesive molecules. In biology, adhesive molecules are found abundantly in the extracellular matrix (ECM) that provides a binding platform for cells [34]–[36]. Examples of ECM molecules are collagen, elastin, fibronectin and laminin. Numerous cell types in the human body communicate and coordinate their behavior by secreting and degrading ECM molecules, namely by modifying the properties of the ECM.

B. Leader-Follower-Based Model of Mobile Communication Networks

The proposed leader-follower-based model (LF model) of mobile molecular communication networks assumes two types of autonomous and mobile bio-nanomachine – leader and follower – that cooperate to control the spatial distribution of bio-nanomachines in a self-organized manner (Fig. 1).

- Leader bio-nanomachines distribute in the environment to detect a target. Upon detecting a target, leader bio-nanomachines release attractant molecules while continuing to move in the environment.
- Follower bio-nanomachines move in the environment and detect attractant molecules. In the presence of attractant molecules, follower bio-nanomachines move preferentially to higher attractant concentrations where they perform application-dependent functionalities. For example, in drug delivery applications (i.e., delivery of drug molecules to target cancer cells), they may carry drug molecules and release the drug molecules at target locations.

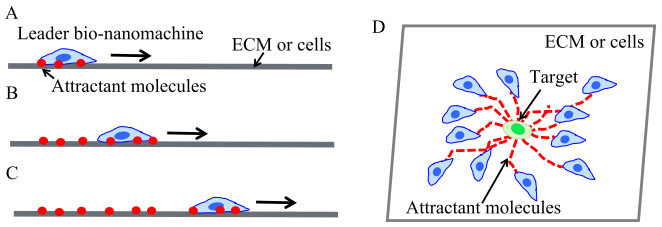

Fig. 2. Attractant gradient formation by leader bio-nanomachines.

The LF model described in this paper uses an adhesive type of attractant molecule, such that bio-nanomachines use non-diffusion-based molecular communication. Attractant molecules released by leader bio-nanomachines bind to the surface of an environment and remain where they are released (Fig. 2A). A trail of attractant molecules is formed as a leader bio-nanomachine moves within the environment (Fig. 2B and C). When a multitude of attractant trails have been formed, an attractant gradient is established in such a manner that the concentration is the highest around the target and decreases with distance thereof (Fig. 2D). In this case, follower bio-nanomachines move according to with the attractant gradient toward the target. In biology, directed cell migration due to surface-bound adhesive molecules is called haptotaxis whereas that through diffusive molecules is called chemotaxis [24], [25]. The use of adhesive molecules has several advantages over diffusive molecules [16]; for example, the attractant concentration may not be impacted by flow in the environment (e.g., blood flows in blood vessels and flows in tissue fluids); the attractant concentration remains high for a long period of time, thus allowing bio-nanomachines to accurately detect the concentration.

III. Mathematical Models

This section describes mathematically the LF model proposed in this paper. For simplicity, the following is assumed:

- The monitoring environment is two-dimensional and defined as an area A.
- The target exists uniformly in a sub-area A_T ($\subseteq A$) within the monitoring environment.
- Bio-nanomachines do not physically interact with each other; no collisions are considered.

A. Leader Bio-Nanomachines

We use the Langevin equation to describe the mobility of a leader bio-nanomachine. The Langevin equation was used originally to describe the Brownian motion of a particle in a fluid medium.

Let B_l denote a set of leader bio-nanomachines. For each leader bio-nanomachine $b \in B_l$, we have

$$\frac{d^2\vec{X}_b(t)}{dt^2} = -\alpha_L \frac{d\vec{X}_b(t)}{dt} + \beta_L \frac{d\vec{W}(t)}{dt}, \quad (1)$$

where $\vec{X}_b(t)$ is the location of leader bio-nanomachine b at time t, α_L is a positive constant determining resistance to the bio-nanomachine's motion, β_L is a positive constant determining the degree of noise effects on the bio-nanomachine's motion, and $\vec{W}(t)$ is the vector Wiener process (noise effects), which has the property that $\vec{W}(t) - \vec{W}(s)$ is Gaussian distributed with a mean of zero and variance of $|t-s|$ where t and s are any two time instances.

A leader bio-nanomachine is either in the active state releasing $M(>0)$ attractant molecules (unit quantity per unit time) or in the inactive state not releasing attractant molecules according to the following:

- Leader bio-nanomachine b $(\in B_l)$ in the target area $(\vec{X}_b(t) \in A_T)$ releases attractant molecules.
- Leader bio-nanomachine b $(\in B_l)$ outside the target area $(\vec{X}_b(t) \notin A_T)$ releases attractant molecules if it recently visited the target area, namely, if the time elapsed since its most recent visit to the target area is within the attractant release time duration T. Leader bio-nanomachine b outside the target area does not release attractant molecules if it never visited the target area.

Note that the behavior assumed above for leader bio-nanomachines may be implemented from smart materials [37]. For instance, bio-nanomachines made from smart materials change the permeability of their surfaces according to the environmental conditions (e.g., pH level) and release (or not) stored molecules (attractant molecules) through their surfaces. How quickly they change the permeability (indicating the time duration T) depends on the chemical composition of the bio-nanomachines, which can be tuned to control the time duration T. Further, clock-like behaviors can be found in biological cells (i.e., biological oscillators [38]); in addition, synthetic biologists have demonstrated that such behavior can occur in engineered bacteria [39]. Clock-like behavior may also be used to control the time duration T when biological cells are used as bio-nanomachines.

B. Attractant Concentration

Attractant molecules released by leader bio-nanomachines remain where they are released. Attractant molecules do not diffuse as they are assumed to be adhesive and bind to the surface of the monitoring environment. The number of attractant molecules in the environment decays with time. Let $c(\vec{x}, t)$ denote the surface concentration of attractant molecule at location $\vec{x}$ and time t. Then the rate of change in $c(\vec{x}, t)$ is given by a partial differential equation:

$$\frac{\partial c(\vec{x}, t)}{\partial t} = \sum_{b \in B_a(t)} M\delta(\vec{x} - \vec{X}_b(t)) - kc(\vec{x}, t), \quad (2)$$

where $B_a(t)$ is the set of active leader bio-nanomachines at time t, M is the attractant release rate, $\delta(\cdot)$ is the Dirac delta function expressing the locations where leader bio-nanomachines release attractant molecules, and k is the degradation rate constant of the attractant molecule. Note that (2) is consistent with how the dynamics of ECM molecules is modeled in the literature [40], [41].

C. Follower Bio-Nanomachines

We also use the Langevin equation to describe the mobility of follower bio-nanomachines. Let B_f denote a set of follower bio-nanomachines. For each follower bio-nanomachine $b \in B_f$, we have

$$\frac{d^2\vec{X}_b(t)}{dt^2} = -\alpha_F \frac{d\vec{X}_b(t)}{dt} + \beta_F \frac{d\vec{W}(t)}{dt} + \gamma \ \nabla c(\vec{x}, t)|_{\vec{x}=\vec{X}_b(t)},$$

where α_F is a positive constant determining the resistance to the bio-nanomachine's motion, β_F is a positive constant determining the degree of noise effects on the bio-nanomachine's motion, γ is a positive constant determining the impact of the attractant concentration gradient $\nabla c(\vec{x}, t)$ at location $\vec{x} = \vec{X}_b(t)$ on the directional motion of bio-nanomachine b and $\nabla = \vec{e}_x \frac{\partial}{\partial x} + \vec{e}_y \frac{\partial}{\partial y}$.

IV. Parameter Estimation

This section describes our wet laboratory experiments and the methods used to estimate parameter values in (1) and (3) from experimental results. The parameter values estimated in this section will be used in Section V to examine the application-level performance of mobile molecular communication networks based on the LF model.

A. Wet Laboratory Experiments

In wet laboratory experiments, we used endothelial cells as a model of bio-nanomachines and fibronectin as the attractant molecule since endothelial cells appear to move up fibronectin gradients [42], [43]. As detailed below, we obtained trajectories of cells in the presence and absence of fibronectin gradients in order to obtain α_L, β_L, α_F, β_F and γ.

Cell Culture: Calf pulmonary artery endothelial (CPAE) cells were obtained from the Institute for Fermentation, Osaka. Cells were cultured in Dulbecco's Modified Eagle Medium (DMEM) supplemented with 20% fetal calf serum (Gibco) at 37 °C under 5% CO_2.

Fibronectin Gradient Formation: The fibronectin gradient was established according to the method described in [44]. Briefly, polydimethylsiloxane (PDMS) was used to form 22 mm (length) × 1 mm (width) × 0.1 mm (depth) microchannels sandwiched between two coverslips. The fibronectin solution containing 10 μg/ml Rhodamine conjugated fibronectin (Cytoskelton, Inc.) in distilled water was then prepared, and microchannels were filled with this solution by capillary force. Finally, the sandwiched michrochannels were placed upright and the fibronectin solution in microchannels was air-dried at 4 °C to create a gradient coating.[2] A fluorescence

[2]In this process, fibronectin-containing DI-water is allowed to air-dry from the opening inlet of a microchannel. Thus, the amount of water decreases over time and the concentration of fibronectin increases accordingly. Since the microchannel is placed upright during the coating process, gravity would drag liquid down in the microchannel. In this way, the surface that is close to the top of the microchannel will have lowest deposition of fibronectin since the concentration was low and the overall time that the surface is exposed to the coating solution is also short. On the other hand, the area close to the bottom will have higher coating concentration since the overall coating time is longer and the fibronectin concentration is also increased gradually over time. Once the DI-water is completely air-dried, the coating process is complete.

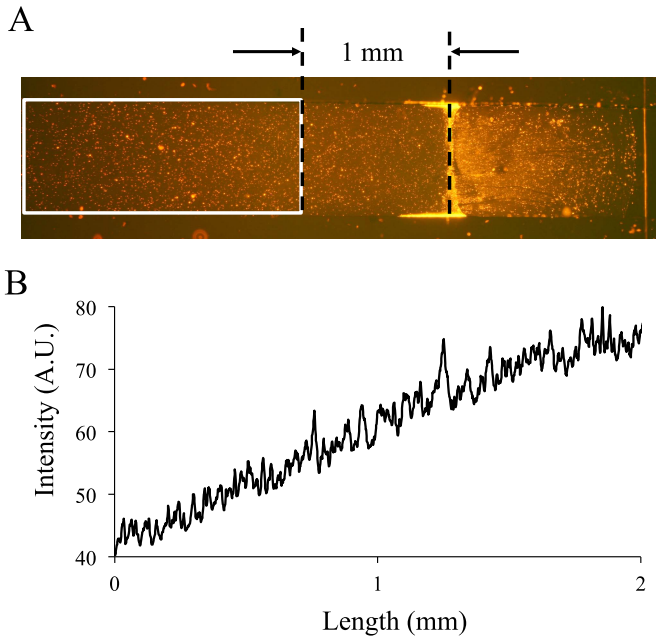

Fig. 3. Rhodamine-conjugated fibronectin gradient. (A) Fluorescence microscopy image of a microchannel where the gradient is formed. The fluorescence intensity of rhodamine was measured at 535 nm/585 nm for excitation/emission wavelengths. (B) The fluorescence intensity of rhodamine in the square area in A is shown.

microscope was used to examine the fibronectin gradients on the coverslip (Fig. 3A and B) before they were used in time-lapse imaging experiments.

Time-Lapse Imaging: Prior to time-lapse imaging experiments, coverslips were placed in plastic dishes to which cells were transfered and incubated for at least 2 hours under the same cell culture conditions. Time-lapse imaging was then performed using an Olympus CKX41 microscope with a 10× objective lens in a temperature-controlled room at 37 °C. Images were taken every minute for 12 hours or longer, with each image capturing an area of approximately 1.2 mm × 1.5 mm of coverslip.

Obtaining Cell Trajectories: ImageJ software [45] and MTrackJ plugin [46] were used to monitor cell trajectories. Cells that neither collided with other cells nor commenced cell division were selected and their locations were identified manually by center of mass. The locations of selected cells were identified every 10 min from time-lapse imaging, such that 73 locations per selected cell were identified from 12 hours of imaging to define cell trajectories.

Fig. 4 shows images of a selected cell which moved preferentially to the higher fibronectin concentration. Figs. 5A and B show the trajectories of two selected cells. Here the cell's initial position is the origin of the two-dimensional space, with increasing fibronectin concentration shown along the x-axis; the cell in Fig. 5A exhibited a more preferential movement towards the higher fibronectin concentration than the cell in Fig. 5B. For comparison, Fig. 5C shows the trajectory of a cell that was placed on a coverslip without fibronectin.

B. Maximum Likelihood Estimation

Each trajectory of a cell is given as a sequence $((x_n, y_n))_{n=1}^{N}$ of the cell's locations on a two-dimensional surface, where N is the number of locations obtained from experiments. In experiments, the cell's location was measured every 10 min over 12 hours, yielding a sequence of $N = 73$ locations.

Given a cell's trajectory obtained from time-lapse imaging, we use the maximum likelihood estimation (MLE) to estimate α_F, β_F, γ in (3) for follower bio-nanomachines. We assume that leader bio-nanomachines are developed from the same cell type and have the same parameter values: namely, $\alpha_F = \alpha_L$ and $\beta_F = \beta_L$, respectively denoted as α and β in the rest of the paper, to simplify the expressions.

We first rewrite (3) as

$$\frac{d^2x(t)}{dt^2} = -\alpha\frac{dx(t)}{dt} + \beta\frac{dW_x(t)}{dt} + \gamma', \tag{3}$$

$$\frac{d^2y(t)}{dt^2} = -\alpha\frac{dy(t)}{dt} + \beta\frac{dW_y(t)}{dt}, \tag{4}$$

where the fibronectin gradient is assumed to be made linearly along the x-axis and γ' $(= \gamma\frac{\partial c}{\partial x})$ is a constant determining the directional force that directs cells to move along the x-axis.

We then discretize (3) and (4) by time interval τ with respect to time t:

$$\frac{x_{i+2} - 2x_{i+1} + x_i}{\tau^2} = -\alpha\frac{x_{i+1} - x_i}{\tau} + \beta R_{x_i} + \gamma', \tag{5}$$

$$\frac{y_{i+2} - 2y_{i+1} + y_i}{\tau^2} = -\alpha\frac{y_{i+1} - y_i}{\tau} + \beta R_{y_i}, \tag{6}$$

where $R_{x_i} = \dfrac{W_{x_{i+1}} - W_{x_i}}{\tau}$ and $R_{y_i} = \dfrac{W_{y_{i+1}} - W_{y_i}}{\tau}$. R_{x_i} and R_{y_i} are white noise and independent of i; hence we write $R_{x_i} = R_{y_i} \equiv R \sim \mathcal{N}(0, \frac{1}{\tau})$.

By shifting the time index i by -2 in (5) and (6), we can obtain

$$\hat{x}_i = \tau^2\beta R - \alpha\tau\,(x_{i-1} - x_{i-2}) + 2x_{i-1} - x_{i-2} + \tau^2\gamma', \tag{7}$$

$$\hat{y}_i = \tau^2\beta R - \alpha\tau\,(y_{i-1} - y_{i-2}) + 2y_{i-1} - y_{i-2}, \tag{8}$$

where $\hat{x}_i$ and $\hat{y}_i$ are used to express the estimated locations given x_{i-1}, x_{i-2}, y_{i-1} and y_{i-2}.

Notice in (7) and (8) that $\hat{x}_i$ and $\hat{y}_i$ are both linear functions of $R \sim \mathcal{N}(0, \frac{1}{\tau})$; the probability density functions of $\hat{x}_i$ and $\hat{y}_i$ are given by

$$\hat{x}_i \sim P_{\hat{x}_i}(x) = \frac{1}{\sqrt{2\pi\sigma^2}}\exp\left(-\frac{(x - \bar{x}_i)^2}{2\sigma^2}\right), \tag{9}$$

$$\hat{y}_i \sim P_{\hat{y}_i}(y) = \frac{1}{\sqrt{2\pi\sigma^2}}\exp\left(-\frac{(y - \bar{y}_i)^2}{2\sigma^2}\right), \tag{10}$$

where

$$\bar{x}_i = -\alpha\tau\,(x_{i-1} - x_{i-2}) + 2x_{i-1} - x_{i-2} + \tau^2\gamma',$$

$$\bar{y}_i = -\alpha\tau\,(y_{i-1} - y_{i-2}) + 2y_{i-1} - y_{i-2},$$

$$\sigma^2 = \beta^2\tau^3.$$

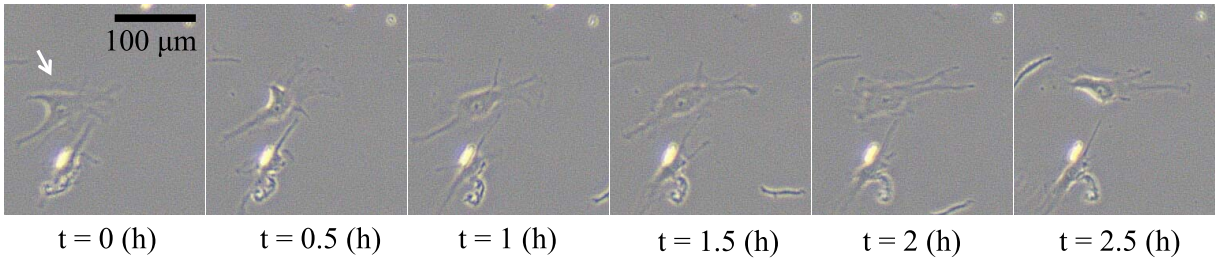

Fig. 4. Microscopy images of a CPAE cell. The fibronectin concentration increases from left to right in each image. The cell indicated by the arrow moved to the higher fibronectin concentration.

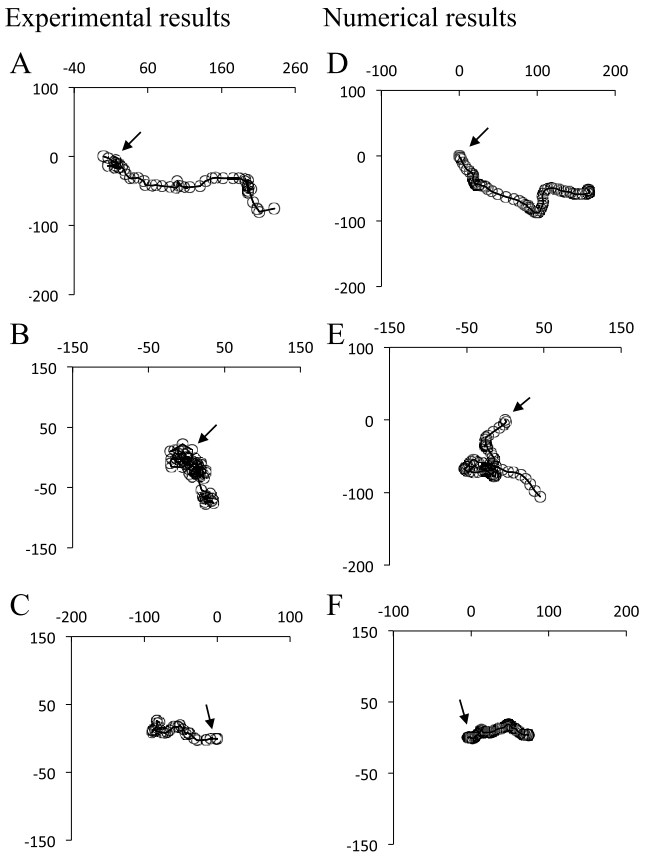

Fig. 5. Trajectories of cells moving on a gradient substrate (A and B), and on a non-gradient substrate (C), each obtained from 12 hours of time-lapse imaging. On the gradient substrate, the fibronectin concentration increases from left to right. The cell's starting position is the origin of the two-dimensional coordinate and indicated by the arrow. Parameter values estimated from trajectories A-C are used to produce trajectories D-F. Axis unit is μm.

With (9) and (10), the joint probability density function $P_i(x, y)$ is written as

$$P_i(x, y) = P_{\hat{x}_i}(x) \cdot P_{\hat{y}_i}(y). \tag{11}$$

The log likelihood of obtaining the sequence $((x_i, y_i))_{n=3}^{N}$ is then given as

$$L(\alpha, \beta, \gamma') = \sum_{n=3}^{N} \ln P_n(x_n, y_n). \tag{12}$$

To obtain the maximum likelihood estimates of α, β and γ' that maximize the likelihood function (12), we solve the simultaneous equations below.

$$\begin{cases} \dfrac{\partial L(\alpha, \beta, \gamma')}{\partial \alpha} = 0 \\ \dfrac{\partial L(\alpha, \beta, \gamma')}{\partial \beta} = 0 \\ \dfrac{\partial L(\alpha, \beta, \gamma')}{\partial \gamma'} = 0 \end{cases} \tag{13}$$

C. Results and Discussion

We applied the MLE method to the trajectories of 10 cells obtained from time-lapse imaging experiments and estimated parameter values (Table I). Further, we used estimated parameter values to reproduce trajectories. From the trajectory shown in Fig. 5A, parameter values listed for Cell 1 in Table I were estimated, and used to produce the trajectory shown in Fig. 5D. Similarly, from the trajectory in Fig. 5B, parameter values listed listed for Cell 5 in Table I were estimated and used to produce the trajectory in Fig. 5E. As shown in these figures, the reproduced results are in good agreement with experimental results.

In Table I, the variance of γ' is large compared to that of α and β. There are several reasons for this. First, biological cells always present variability. Some cells do not have the ability to respond to the fibronectin gradient (i.e., haptotactic response). For practical use, we will be selecting cells for specific applications. Also, it should be noted that cell migration depends on the cell cycle phase; we observed in experiments that cells stop migrating when they enter cell division. The variance may be reduced if the model is refined by considering the cell cycle. Finally, the engineered fibronectin gradient is not smooth. As shown in Fig. 3, the fibronectin concentration (y-axis value) increases with the x-axis value at a relatively constant rate, but it fluctuates. This introduces location-dependency into the cell's haptotactic response. This should be solvable as the engineering techniques advance.

To understand the mobility of these cells, we computed the following quantities that dictate the speed S_{drift} of directional motion along the fibronectin gradient and the speed S_{rand} of random motion

$$S_{drift} = \frac{\gamma'}{\alpha},$$
$$S_{rand} = \frac{\beta}{\sqrt{\alpha}}.$$

TABLE I
ESTIMATED PARAMETER VALUES

Cell	α [h^{-1}]	β [$\mu m\ h^{-\frac{3}{2}}$]	γ' [$\mu m\ h^{-2}$]	S_{drift} [$\mu m\ h^{-1}$]	S_{rand} [$\mu m\ h^{-1}$]
1	0.57	2.90	1.51	2.66	3.85
2	0.48	2.98	0.80	1.67	4.31
3	0.56	3.23	-1.61	-2.85	4.37
4	0.46	3.24	-0.27	-0.60	4.80
5	0.55	3.52	0.21	0.38	4.73
6	0.53	3.39	-0.13	-0.26	4.67
7	0.42	3.53	0.36	0.85	5.42
8	0.62	3.89	0.13	0.21	5.01
9	0.53	3.15	0.36	0.68	4.34
10	0.40	2.76	0.38	0.94	4.34
Mean $\pm$ SEM	0.51 $\pm$ 0.07	3.27 $\pm$ 0.34	0.17 $\pm$ 0.80	0.37 $\pm$ 1.47	4.59 $\pm$ 0.44

TABLE II
SUMMARY OF ESTIMATED PARAMETER VALUES

Experimental setup	α [h^{-1}]	β [$\mu m\ h^{-\frac{3}{2}}$]	S_{rand} [$\mu m\ h^{-1}$]
No FN	0.47 $\pm$ 0.02	1.41 $\pm$ 0.08	2.08 $\pm$ 0.12
FN (Uniform: low)	0.46 $\pm$ 0.03	1.16 $\pm$ 0.09	1.73 $\pm$ 0.16
FN (Uniform: middle)	0.56 $\pm$ 0.02	0.97 $\pm$ 0.08	1.30 $\pm$ 0.11
FN (Uniform: high)	0.28 $\pm$ 0.02	0.87 $\pm$ 0.06	1.68 $\pm$ 0.13

As shown in Table I, the mean of S_{drift} is a magnitude smaller than the mean of S_{rand}, demonstrating the degree to which cells moved randomly even in the presence of fibronectin gradients.

The parameter values α and β can also be estimated from time-lapse imaging experiments with fibronectin-uncoated (a) and coated (b) coverslips. We performed these additional experiments and applied the MLE method. Table II summarizes the estimated parameter values from each experimental setup; "No FN" refers to experimental setup (a), while "FN (Uniform: low)", "FN (Uniform: middle)" and "FN (Uniform: high)" refer to experimental setup (b), where three different levels of fibronectin concentrations were tested. In each experimental setup, 10 cells were examined. An example cell trajectory obtained from "No FN'' is shown in Fig. 5C, with parameter values estimated from this figure used to produce the trajectory shown in Fig. 5F.

Table II shows that α and β values differ depending on the experimental setup, meaning that they are influenced by the fibronectin concentration. This suggests that the mathematical models could be improved by incorporating the fibronectin concentration therein (e.g., (3)), in addition to the fibronectin gradient. Table II also shows that S_{rand} tends to decrease when the fibronectin concentration is increased (e.g., from 0 to high). This is understandable since the increased binding force between cells and the environment surface can decrease the cell mobility. By comparing S_{rand} in Tables I and II, it is also seen that S_{rand} is large in the presence of fibronectin gradients (i.e., S_{rand} is larger in Table I than in Table II). This increase in S_{rand} may be caused by the fact that the fibronectin gradients were bumpy (Fig. 3); this may have accelerated the random motion of cells.

V. SIMULATION EXPERIMENTS

In simulation experiments, we evaluate the application-level performance of mobile molecular communication networks designed based on the LF model. For comparison, we consider the *all-in-one* model where single bio-nanomachines implement all necessary functionalities such as detecting targets, releasing attractant molecules, and migrating to the higher attractant concentration in the environment. In the all-in-one model, bio-nanomachines release attractant molecules as leader bio-nanomachines do (see Section $III-A$) and migrate in the same manner as follower bio-nanomachines migrate according to (3). The concentration of attractant molecule is governed by (2).

A. Simulation Scenario

We consider an application of mobile molecular communication networks to tumor site detection in the human body. Tumor cells may exist in the human body for many years before they start to metastasize [47]. Based on current radiological methods, tumor cells are detected after they grow to a detectable level (a few mm), which is estimated to be 10 – 15 years after the first tumor cell was born. At this stage, metastasis have often formed, and cancer therapies may not be effective. Based on this observation, tumor site detection within a few years is assumed to be a practical objective.

In the all-in-one model, we use N_b bio-nanomachines. In the LF model, we use N_l leader bio-nanomachines and N_f follower bio-nanomachines. We then assume that, for the purpose of tumor site detection, imaging probes [48] are loaded onto all bio-nanomachines in the all-in-one model and onto follower bio-nanomachines in the LF model. As a performance metric, we use the likelihood $R_T(t)$ that the tumor site is detected at time t:

$$R_T(t) = \frac{|B_{IP}|}{d_{AVG}(t)}, \tag{14}$$

where $|B_{IP}|$ is the number of bio-nanomachines carrying the imaging probes (i.e., N_b in the all-in-one model and N_f in the LF model) and $d_{AVG}(t)$ is the average distance between a bio-nanomachine and the target site at time t. $R_T(t)$ increases as $|B_{IP}|$ increases and $d_{AVG}(t)$ decreases. In simulation experiments described in this section, we examine how $R_T(t)$ changes over time. We also examine $R_T(t)$ after a sufficiently long period of time $\bar{t}$ (= 1, 2 or 3 years) elapses. As a performance metric, we use $\bar{R}_T$, the average of $R_T(\bar{t})$ computed from 10 simulation runs.

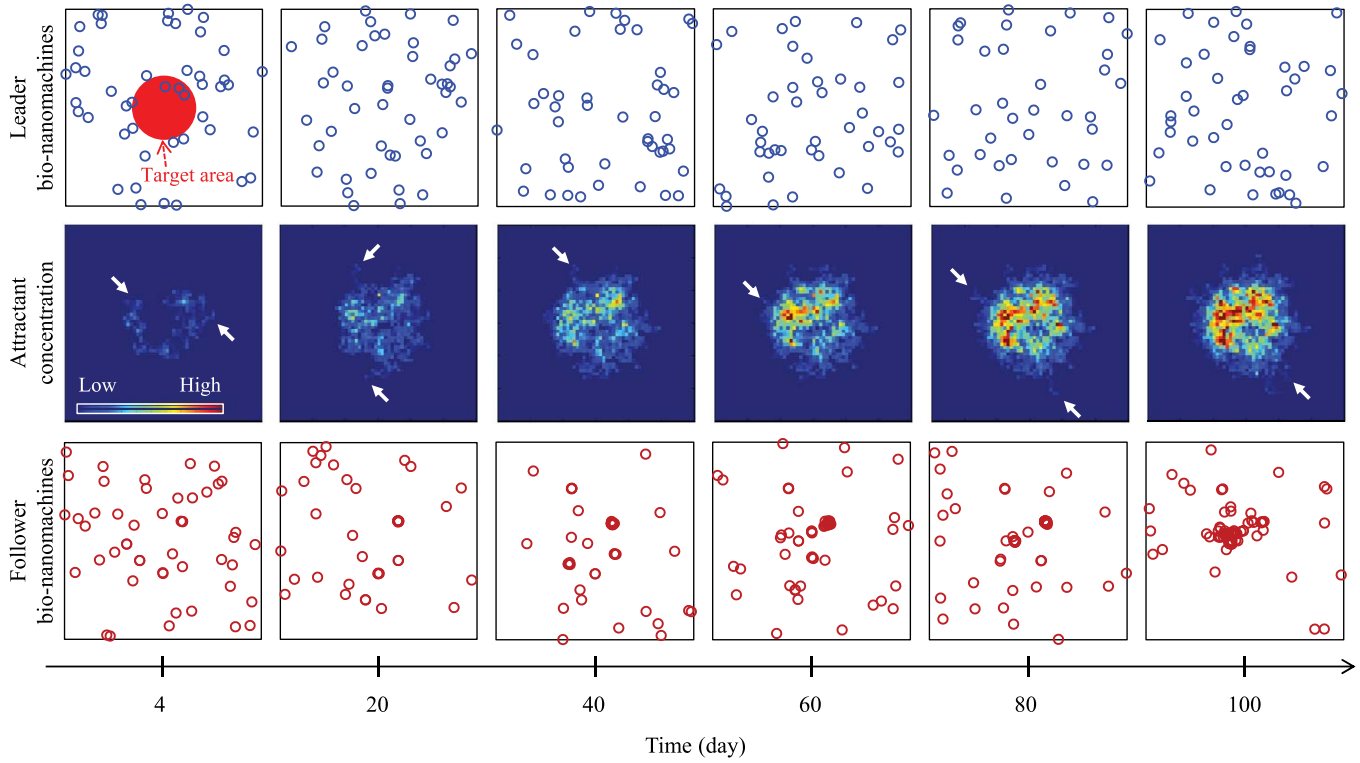

Fig. 6. An example simulation run when the LF model is used. Leader bio-nanomachine distribution (top), attractant concentration (middle), and follower bio-nanomachine distribution (bottom) are shown. Each image shows a 6 (mm) × 6 (mm) area of the 20 (mm) × 20 (mm) monitoring area. The target area is circular, 1 (mm) in radius and at the center of the monitoring area as shown in the top left image. Leader and follower bio-nanomachines are represented by circles. The attractant concentration is indicated by color coding. Arrows in the attractant concentration point to attractant trails.

B. Parameter Values

The monitoring environment is an $L \times L$ square area defined as $A = \{(x, y)| -\frac{L}{2} \leq x \leq \frac{L}{2}, -\frac{L}{2} \leq y \leq \frac{L}{2}\}$ with $L = 20$ (mm), representing the tissue space shown in Fig. 1. The target area is circular and positioned at the center of the monitoring environment, and it is defined as $A_T = \{(x, y)|x^2 + y^2 \leq L_T^2\}$ with $L_T = 1$ (mm). This target area indicates that 10^6 tumor cells exist in the area when a tumor cell of 10 μm in radius is assumed. [3] If we further assume slow-growing tumor cells with their doubling time of 6 months, it takes approximately 10 years for a single tumor cell to grow into this size.

For α, β and γ, we use the values of Cell 1 in Table I. Note that γ is determined based on cell 1's γ' in Table I, the relationship of $\gamma' = \gamma \frac{dC_x}{dx}$, and the experimentally measured value of $\frac{dC_x}{dx} = 0.02$ (A.U./μm).

Other values are arbitrarily determined. Unless otherwise noted, the number of bio-nanomachines is $N_b = 1000$ for the all-in-one model, and $N_l = N_f = 500$ for the LF model. The attractant release rate is $M = 0.1$ (A.U./h), the attractant release time duration is $T = 216$ (h), and the attractant degradation rate constant is $k = 1 \times 10^{-5}$ (1/h).

At time $t = 0$, bio-nanomachines are randomly distributed in the monitoring environment. All these bio-nanomachines have zero moving velocities at $t = 0$. During the course of the simulation runs, bio-nanomachines are not allowed to move outside the monitoring environment, rebounding back into the monitoring environment when they make contact with the environment boundaries. In solving (2), the monitoring environment is divided into 0.1×0.1 (mm^2) square areas. Time t in (1), (2) and (3) is discretized by $\Delta t = 1$ (min), and each simulation run is terminated when time $t = 50,000$ (h) ($\sim$5.7 years) is reached. At each simulation time step, $d_{AVG}(t)$ in (14) is computed as the averaged distance between a bio-nanomachine and the center of the target area (i.e., the origin of the coordinate space).

Fig. 6 shows when the LF model is used with the parameter values described above. It shows how the attractant concentration, leader bio-nanomachine distribution and follower bio-nanomachine distribution evolve with time. Note that the monitoring area is 20 (mm) × 20 (mm) and each image in Fig. 6 shows the 6 (mm) × 6 (mm) area of the monitoring area. As shown in the top series of images, leader bio-nanomachines remain distributed in the environment. The target area is circular as shown in the top left image in Fig. 6, whereon leader bio-nanomachines that enter this area release attractant molecules. The leader bio-nanomachines that release attractant molecules continue to move in the environment, leading to the formation of attractant concentration gradients (middle series of images). Since attractant molecules are assumed in this paper to be adhesive and not diffusive, the

[3]The number of tumor cells in the target area is estimated from the volume of the target divided by the volume of a tumor cell.

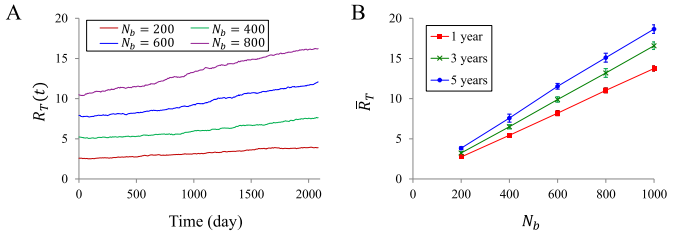

Fig. 7. Impact of N_b on $R_T(t)$ and $\bar{R}_T$ in the all-in-one model.

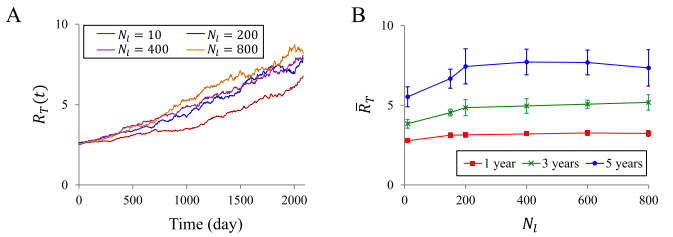

Fig. 8. Impact of N_l on $R_T(t)$ and $\bar{R}_T$ in the LF model. $N_f = 200$.

attractant concentration tends to form trails (see arrows in the attractant concentration images). As more leader bio-nanomachines release attractant molecules and move in the environment, attractant trails overlap and the attractant gradient is formed. The attractant concentration is high in the target area and tends to decrease with distance from it. This formation of the attractant concentration gradient allows follower bio-nanomachines to move closer to the target area. As shown in the lower series of images, follower bio-nanomachines are gradually attracted to the target area.

C. Results: Impact of the Number of Bio-Nanomachines

Fig. 7 shows the impact of the number of bio-nanomachines N_b on $R_T(t)$ and $\bar{R}_T$ when the all-in-one model is used. As shown in Fig. 7B, $\bar{R}_T$ increases almost linearly with N_b. From (14), it is seen that $R_T(t)$ increases linearly with N_b if $d_{AVG}(t)$ is a constant and not influenced by N_b. The linear relationship between N_b and $\bar{R}_T$ observed in Fig. 7B indicates that $d_{AVG}(t)$ is not influenced by N_b, implying that the effective attractant gradient is formed in all cases tested and bio-nanomachines are effectively directed to the target area.

On the other hand, Figs. 8 and 9 show $R_T(t)$ and $\bar{R}_T$ when the LF model is used; in Fig. 8, N_l is varied and $N_f = 200$, whereas in Fig. 9, N_f is varied and $N_l = 200$. Fig. 8B shows that $\bar{R}_T$ slightly increases as N_l increases from 10 to 200; however, it does not increase further with N_l. This indicates that 200 leader bio-nanomachines are sufficient to create an effective attractant gradient and no further leader bio-nanomachines are required. Fig. 9B shows that $\bar{R}_T$ increases almost linearly with N_f, and this is because the number of leader bio-nanomachines $N_l = 200$ is sufficient to create an effective attractant gradient and thus $\bar{R}_T$ increases linearly with N_f according to (14).

In the LF-model, one practical problem is to identify the optimal numbers of leader and follower bio-nanomachines. Fig. 10 shows $R_T(t)$ and $\bar{R}_T$ for various N_l values in the LF model where the total number of bio-nanomachines is fixed

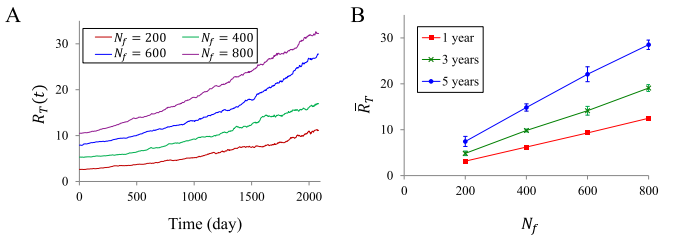

Fig. 9. Impact of N_f on $R_T(t)$ and $\bar{R}_T$ in the LF model. $N_l = 200$.

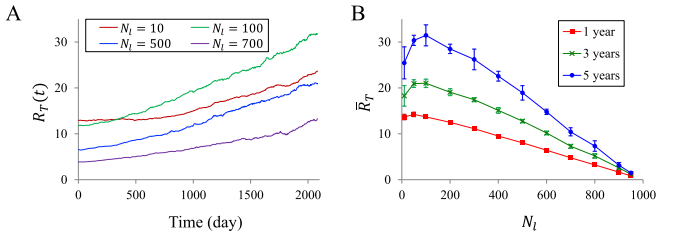

Fig. 10. Impact of N_l on $R_T(t)$ and $\bar{R}_T$ in the LF model. $N_f = 1000 - N_l$.

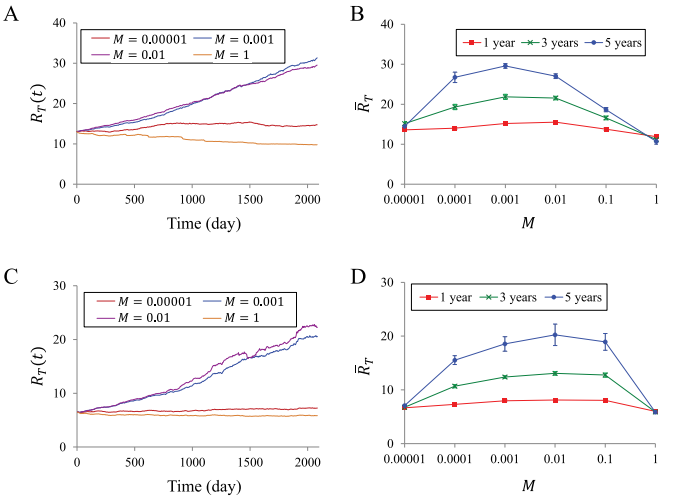

Fig. 11. Impact of M on $R_T(t)$ and $\bar{R}_T$ in the all-in-one model (A and B) and in the LF model (C and D).

to $N_l + N_f = 1000$. These figures show that the optimal ratio of $N_l : N_f$ that maximizes $\bar{R}_T$ exists at $N_l : N_f = 50 : 950 - 100 : 900$. This optimal ratio exists since, when N_l is too small, the gradient is not formed and follower bio-nanomachines are not attracted to the target area, and when N_l is large, the number of follower bio-nanomachines becomes small, leading to small $\bar{R}_T$. It is observed here that, when the numbers of leader and follower bio-nanomachines are optimized, the LF model can achieve larger $\bar{R}_T$; in the LF model, $N_l = 100$ and $N_f = 900$ result in $\bar{R}_T = 31.5$ at $t = 5$ (years) while in the all-in-one model, the same number of bio-nanomachines $N_b = 1000$ results in $\bar{R}_T = 18.7$ at $t = 5$ (years) (see Fig. 7B).

D. Results: Impact of the Attractant Release Rate

Fig. 11A and B show the impact of the attractant release rate M on $R_T(t)$ and $\bar{R}_T$ when the all-in-one model is used; and Fig. 11C and D show that when the LF model is used.

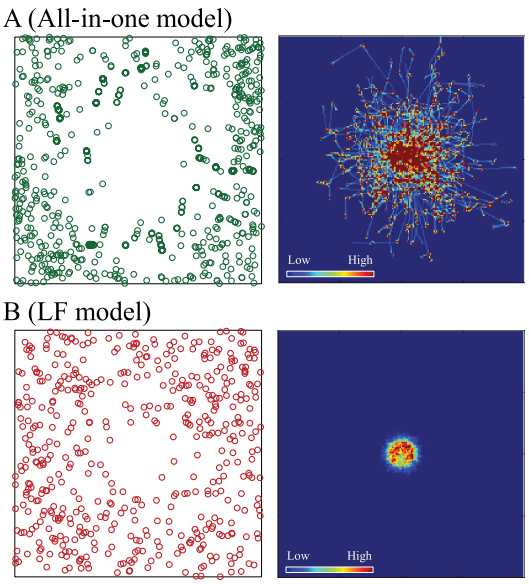

Fig. 12. Bio-nanomachine distribution (left) and attractant concentration distribution (right) in the all-in-one model (A) and the LF model (B). Each image shows the 20 (mm) × 20 (mm) monitoring area. $M = 1$ (A.U./h). $t = 416$ (days).

As shown in these figures, $R_T(t)$ and $\bar{R}_T$ increase and then decrease as M increases from $M = 0.00001$ (A.U./h) in both models.

When M is small, $R_T(t)$ does not increase with time t (see the $M = 0.00001$ case in Fig. 11A and C). This is because attractant molecules released by bio-nanomachines are too low in concentration (or intensity) and degrade before effective gradients are formed. In such cases, bio-nanomachines remain almost uniformly distributed in the area during simulation runs (data not shown), and $R_T(t)$ does not increase with time t.

It is also seen that, when M is large, $R_T(t)$ does not increase with time t (see the $M = 1$ case in Fig. 11A and C). For this reason, we observed that, when M is large, bio-nanomachines stay around the target area while not many are found within the target area; see Fig. 12A left for the all-in-one model and Fig. 12B left for the LF model. This is likely because the moving velocities of bio-nanomachines become too large as the attractant gradient is very large around the target area, and bio-nanomachines pass through the target area. This prevents bio-nanomachines from staying in the proximity of the target area and reduces $R_T(t)$ and $\bar{R}_T$. When $M = 1$ (A.U./h), by comparing the two models, we observed that the attractant distribution differs significantly in the two models. In the all-in-one model, the attractant concentration exhibits a spider-web-like complex distribution with attractant trails formed in a wide area (Fig. 12A right), while in the LF model, the attractant concentration is distributed in a Gaussian-like distribution in a small area (Fig. 12B right). The attractant concentration in the LF model is simple because leader bio-nanomachines keep moving randomly to create an attractant gradient, while in the all-in-one model bio-nanomachines move based on the attractant gradient that they create in creating an attractant gradient. This suggests that system behavior is more predictable with the LF model.

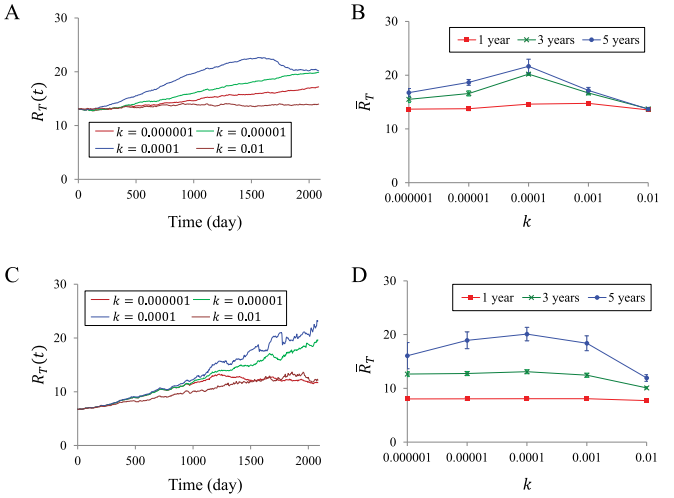

Fig. 13. Impact of k on $R_T(t)$ and $\bar{R}_T$ in the all-in-one model (A and B) and in the LF model (C and D).

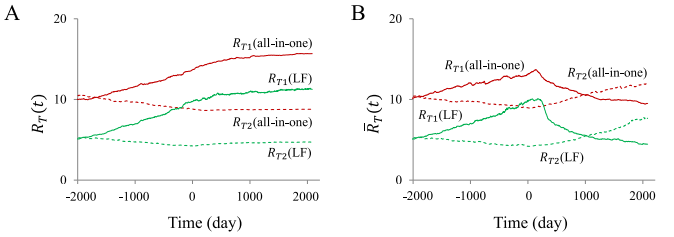

Fig. 14. The target location changes at time $t = 0$ (h). (A) $k = 0.0001$ and (B) $k = 0.0005$.

E. Results: Impact of the Attractant Degradation Rate Constant

Figs. 13A and B show the impact of the attractant degradation rate constant k on $R_T(t)$ and $\bar{R}_T$ in the all-in-one model; and Figs. 13C and D show that when the LF model is used. Similar to the previous case where M is varied, $\bar{R}_T$ increases and then decreases when k is increased from 0.000001 (1/h) in the two models. When k is small, which corresponds to cases where M is large, the attractant gradient around the target area becomes too high and this accelerates the moving velocities of bio-nanomachines, and bio-nanomachines are not able to stay in the proximity of the target area. When k is large, which corresponds to cases where M is small, attractant molecules released by bio-nanomachines degrade quickly and attractant gradients cannot be formed around the target area. Therefore, $\bar{R}_T$ becomes small when k is small or large.

F. Results: Target Relocation

Finally, we consider a dynamic environment where the target area changes during a simulation run and demonstrate that the spatial distribution of bio-nanomachines changes accordingly. A simulation is run with the target area of $A_{T1} = \{(x, y)|(x-5)^2 + (y-5)^2 \leq L_T^2\}$ for the first 50,000 (hours), and then with the target area $A_{T2} = \{(x, y)|(x+5)^2 + (y+5)^2 \leq L_T^2\}$ for the last 50,000 (hours), thus simulating the situation that the target area changes from A_{T1} to A_{T2}. The time at which the target area changes is set to be $t = 0$ (day).

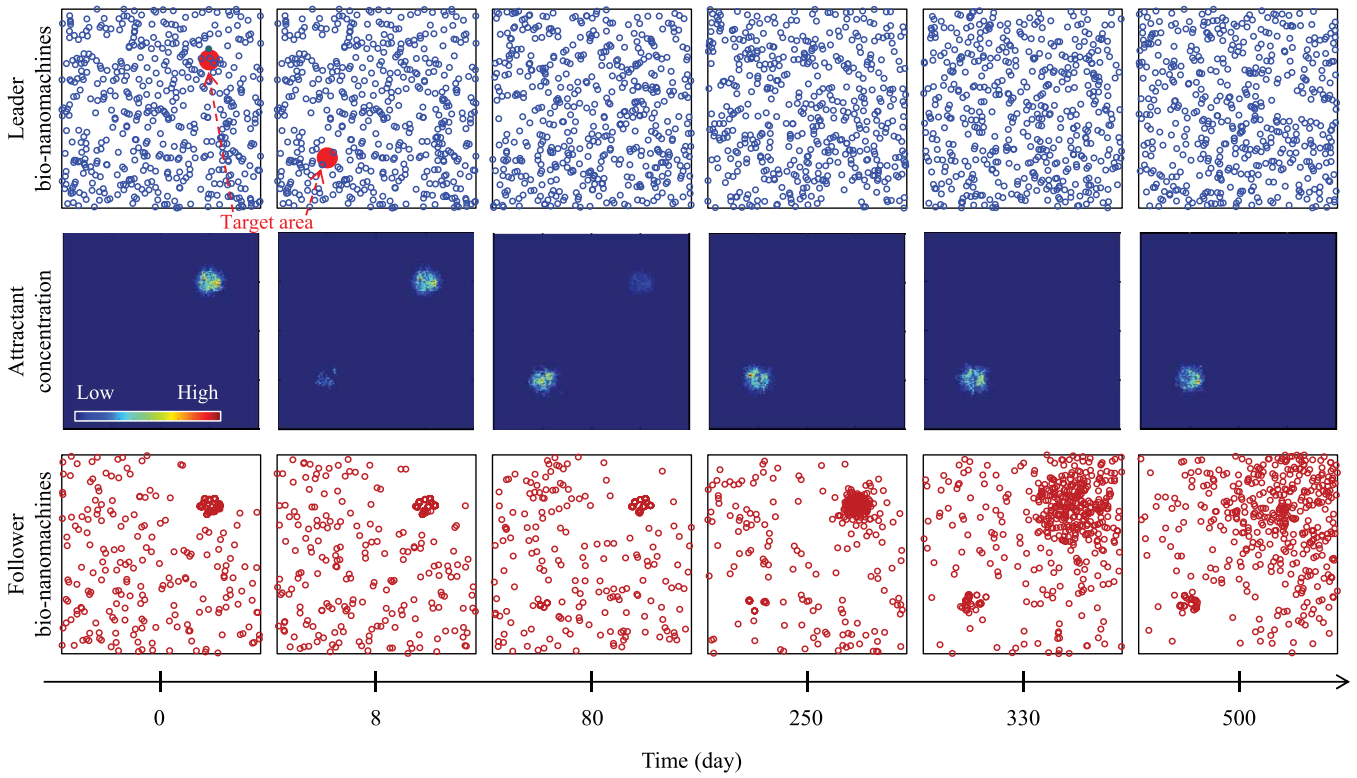

Fig. 15. Leader bio-nanomachine distribution (top), attractant concentration (middle), and follower bio-nanomachine distribution (bottom) are shown. Each image shows the 20 (mm) × 20 (mm) monitoring area. The target area was changed from the top-right position to the bottom-left position as indicated by the red circles in the two top-left images. After the target area changes, it remains there in the rest of the simulation run. The time at which the target area changes is shown as $t = 0$ (day). The LF model is used.

Here we examine $R_{T1}(t)$ and $R_{T2}(t)$ respectively computed using the averaged distance between a bio-nanomachine to the center of A_{T1} (i.e., $(5, 5)$) and that of A_{T2} (i.e., $(-5, -5)$).

Fig. 14A shows the results obtained from both models where a small k value is used ($k = 0.00001$). As shown in the figure, in both models, $R_{T1}(t)$ increases over time, indicating that attractant gradients are formed around the initial target area A_{T1} and bio-nanomachines (or follower bio-nanomachines) move closer to A_{T1}. At time $t = 0$ (day), the target area changed from A_{T1} to A_{T2}, which has little impact on $R_{T1}(t)$ and $R_{T2}(t)$. This is because, with a small k value, the attractant gradients formed around A_{T1} do not disappear, keeping bio-nanomachines around A_{T1} after the target area changes to A_{T2}. In the all-in-one model, effective attractant gradients are not formed around A_{T2}. In the LF model, attractant gradients are formed around A_{T2} by leader bio-nanomachines, but a large number of follower bio-nanomachines remain around A_{T1} and do not move closer to A_{T2}.

Fig. 14B shows the results obtained from both models where the value of k is increased ($k = 0.0005$). In both models, $R_{T1}(t)$ increases over time until the target area changes. After the target area changes, $R_{T1}(t)$ starts to decrease and $R_{T2}(t)$ starts to increase. This demonstrates the ability of both models to adapt the spatial distribution of bio-nanomachines to the change of the target area. Fig. 15 shows how the distributions of leader bio-nanomachines, attractant molecules, and follower bio-nanomachines in the LF model change before and after the target area changes. As shown in Fig. 15, leader bio-nanomachines are uniformly distributed before and after the target area changes. When the target area changes from A_{T1} to A_{T2}, leader bio-nanomachines around A_{T2} start creating attractant gradients. Accordingly, follower bio-nanomachines start moving toward A_{T2} as shown in the figure.

Note that, when k is too large (e.g., $k \geq 0.01$), $R_{T1}(t)$ and $R_{T2}(t)$ do not increase in either model. This is because, when k is too large, effective attractant gradients cannot be formed, as observed in Fig. 13.

VI. Conclusion

We have described a leader-follower-based model of mobile molecular communication networks for target detection applications. Mathematical models, wet laboratory experiments, and methods to estimate model parameters from wet laboratory experimental results have also been presented, along with simulation experiments to evaluate the target detection performance of the proposed mobile molecular communication networks.

The main contributions made in this paper are summarized below.

- The manner in which functionalities can be sub-divided to permit the design of mobile molecular communication networks has been presented. This provides the basis for further design, such as dividing functionalities across

three or more types of bio-nanomachine for a more-advanced drug delivery process (e.g., by combining the model in [11]).

- The functional division proposed in the paper should have a significant impact on the engineering of bio-nanomachines. Current genetic engineering techniques are limited to the delivery of a small number of genes into a single cell. Adding numerous functionalities is difficult as the expression of inserted genes interferes with other genes or interferes with existing components in the cell. Limiting the number of functionalities to implement per cell is necessary.
- The proposed functional division will have a significant impact on drug delivery applications. In the all-in-one model, drug molecules or imaging probes need to be loaded onto all bio-nanomachines, whereas in the LF-model they can be loaded onto the follower bio-nanomachines only. This reduces the risk of side effects as well as the cost of drug molecules or imaging probes.
- Numerical experiments show that the all-in-one model and LF model differ in terms of sensitivity to parameters. Parameter tuning becomes difficult in the all-in-one-model where bio-nanomachines move based on the attractant gradient that they create; this feedback process makes it difficult to predict system behavior. On the other hand, the system behavior is more straightforward when the LF model is employed.

Future work should be aimed at refining the mathematical models based on wet laboratory experimental results. For more realistic outcomes, it will be necessary to model physical interactions among bio-nanomachines, biochemical mechanisms to produce and release attractant molecules, three-dimensional environments, and the growth and death of bio-nanomachines.

Future work should also include demonstrating target detection applications of the proposed model in a realistic biological environment. In the experimental setup described in this paper, there is no target and the attractant gradient is pre-made. Narrowing the gap between the experimental setting and the practical setting is an important objective. Furthermore, the use of other cell types to satisfy application-dependent requirements is needed. In the case of fast-growing tumor cells undergoing a doubling time of 20 days, the life expectancy of the host might be reduced to just 1 – 2 years [47]. For the detection of such cells, other cell types (e.g., leukocytes) that can move faster need to be considered, along with the design of molecular communication mechanisms that can allow a group of cells to cooperate.

REFERENCES

[1] S. Hiyama *et al.*, "Molecular communication," in *Proc. NSTI Nanotechnol. Conf.*, vol. 3. 2005, pp. 391–394.

[2] I. F. Akyildiz, F. Brunetti, and C. Blázquez, "Nanonetworks: A new communication paradigm," *Comput. Netw.*, vol. 52, no. 12, pp. 2260–2279, Aug. 2008.

[3] S. Hiyama and Y. Moritani, "Molecular communication: Harnessing biochemical materials to engineer biomimetic communication systems," *Nano Commun. Netw.*, vol. 1, no. 1, pp. 20–30, 2010.

[4] T. Nakano, M. J. Moore, F. Wei, A. V. Vasilakos, and J. Shuai, "Molecular communication and networking: Opportunities and challenges," *IEEE Trans. Nanobiosci.*, vol. 11, no. 2, pp. 135–148, Jun. 2012.

[5] T. Nakano, A. W. Eckford, and T. Haraguchi, *Molecular Communication*. Cambridge, U.K.: Cambridge Univ. Press, 2013.

[6] G. Wei, P. Bogdan, and R. Marculescu, "Bumpy rides: Modeling the dynamics of chemotactic interacting bacteria," *IEEE J. Sel. Areas Commun.*, vol. 31, no. 12, pp. 879–890, Dec. 2013.

[7] N. R. Raz, M.-R. Akbarzadeh-T, and M. Tafaghodi, "Bioinspired nanonetworks for targeted cancer drug delivery," *IEEE Trans. Nanobiosci.*, vol. 14, no. 8, pp. 894–906, Dec. 2015.

[8] L. Felicetti, M. Femminella, G. Reali, T. Nakano, and A. V. Vasilakos, "TCP-like molecular communications," *IEEE J. Sel. Areas Commun.*, vol. 32, no. 12, pp. 2354–2367, Dec. 2014.

[9] T. Nakano, Y. Okaie, and A. V. Vasilakos, "Transmission rate control for molecular communication among biological nanomachines," *IEEE J. Sel. Areas Commun.*, vol. 31, no. 12, pp. 835–846, Dec. 2013.

[10] M. Femminella, G. Reali, and A. V. Vasilakos, "A molecular communications model for drug delivery," *IEEE Trans. Nanobiosci.*, vol. 14, no. 8, pp. 935–945, Dec. 2015.

[11] U. A. K. Chude-Okonkwo, R. Malekian, and B. T. S. Maharaj, "Molecular communication model for targeted drug delivery in multiple disease sites: With diversely expressed enzymes," *IEEE Trans. Nanobiosci.*, vol. 15, no. 3, pp. 230–245, Apr. 2016.

[12] Y. Okaie *et al.*, "Cooperative target tracking by a mobile bionanosensor network," *IEEE Trans. Nanobiosci.*, vol. 13, no. 3, pp. 267–277, Sep. 2014.

[13] Y. Chen, P. Kosmas, P. S. Anwar, and L. Huang, "A touch-communication framework for drug delivery based on a transient microbot system," *IEEE Trans. Nanobiosci.*, vol. 14, no. 4, pp. 397–408, Jun. 2015.

[14] Y. Chen, T. Nakano, P. Kosmas, C. Yuen, A. V. Vasilakos, and M. Asvial, "Green touchable nanorobotic sensor networks," *IEEE Commun. Mag.*, to be published.

[15] Y. Okaie, T. Nakano, T. Hara, and S. Nishio, "Autonomous mobile bionanosensor networks for target tracking: A two-dimensional model," *Nano Commun. Netw.*, vol. 5, no. 3, pp. 63–71, Sep. 2014.

[16] T. Obuchi, Y. Okaie, T. Nakano, T. Hara, and S. Nishio, "Inbody mobile bionanosensor networks through non-diffusion-based molecular communication," in *Proc. IEEE Conf. Commun. (ICC)*, Jun. 2015, pp. 1078–1084.

[17] T. Nakano *et al.*, "Leader-follower based target detection model for mobile molecular communication networks," in *Proc. 17th IEEE Int. Workshop Signal Process. Adv. Wireless Commun. (SPAWC)*, Jul. 2016, pp. 1–5.

[18] G. von Maltzahn *et al.*, "Nanoparticles that communicate *in vivo* to amplify tumour targeting," *Nature Mater.*, vol. 10, pp. 545–552, Jun. 2011.

[19] T. M. Allen and P. R. Cullis, "Drug delivery systems: Entering the mainstream," *Science*, vol. 303, no. 5665, pp. 1818–1822, 2004.

[20] C. Alvarez-Lorenzo and A. Concheiro, "Bioinspired drug delivery systems," *Current Opinion Biotechnol.*, vol. 24, no. 6, pp. 1167–1173, 2013.

[21] A. C. Dudley, "Tumor endothelial cells," *Cold Spring Harbor Perspect. Med.*, vol. 2, no. 3, p. a006536, 2012.

[22] T. Nakano, T. Suda, Y. Okaie, M. J. Moore, and A. V. Vasilakos, "Molecular communication among biological nanomachines: A layered architecture and research issues," *IEEE Trans. Nanobiosci.*, vol. 13, no. 3, pp. 169–197, Sep. 2014.

[23] T. Nakano, S. Kobayashi, T. Suda, Y. Okaie, Y. Hiraoka, and T. Haraguchi, "Externally controllable molecular communication," *IEEE J. Sel. Areas Commun.*, vol. 32, no. 12, pp. 2417–2431, Dec. 2014.

[24] H. C. Berg, *Random Walks in Biology*. Princeton, NJ, USA: Princeton Univ. Press, 1993.

[25] P. Friedl and D. Gilmour, "Collective cell migration in morphogenesis, regeneration and cancer," *Nature Rev. Molecular Cell Biol.*, vol. 10, no. 7, pp. 445–457, 2009.

[26] M. E. Ortiz and D. Endy, "Engineered cell-cell communication via DNA messaging," *J. Biol. Eng.*, vol. 6, p. 16, Dec. 2012.

[27] L. C. Cobo and I. F. Akyildiz, "Bacteria-based communication in nanonetworks," *Nano Commun. Netw.*, vol. 1, no. 4, pp. 244–256, 2010.

[28] M. J. Moore and T. Nakano, "Addressing by beacon distances using molecular communication," *Nano Commun. Netw.*, vol. 2, nos. 2–3, pp. 161–173, 2011.

[29] P. Lio and S. Balasubramaniam, "Opportunistic routing through conjugation in bacteria communication nanonetwork," *Nano Commun. Netw.*, vol. 3, no. 1, pp. 36–45, 2012.

[30] B. Alberts, A. Johnson, J. Lewis, M. Raff, K. Roberts, and P. Walter, *Molecular Biology of the Cell*. New York, NY, USA: Garland, 2008.

[31] B. L. Bassler, "How bacteria talk to each other: Regulation of gene expression by quorum sensing," *Current Opinion Microbiol.*, vol. 2, no. 6, pp. 582–587, 1999.
[32] S. Basu, Y. Gerchman, C. H. Collins, F. H. Arnold, and R. Weiss, "A synthetic multicellular system for programmed pattern formation," *Nature*, vol. 434, pp. 1130–1134, Apr. 2005.
[33] L. You, R. S. Cox, III, R. Weiss, and F. H. Arnold, " Programmed population control by cell–cell communication and regulated killing," *Nature*, vol. 428, pp. 868–871, Apr. 2004.
[34] S.-H. Kim, J. Turnbull, and S. Guimond, "Extracellular matrix and cell signalling: The dynamic cooperation of integrin, proteoglycan and growth factor receptor," *J. Endocrinol.*, vol. 209, pp. 139–151, Feb. 2011.
[35] J. M. Rhodes and M. Simons, "The extracellular matrix and blood vessel formation: Not just a scaffold," *J. Cellular Molecular Med.*, vol. 11, no. 2, pp. 176–205, 2007.
[36] L. Felicetti, M. Femminella, G. Reali, P. Gresele, M. Malvestiti, and J. N. Daigle, "Modeling CD40-based molecular communications in blood vessels," *IEEE Trans. Nanobiosci.*, vol. 13, no. 3, pp. 230–243, Sep. 2014.
[37] D. A. LaVan, T. McGuire, and R. Langer, "Small-scale systems for *in vivo* drug delivery," *Nature Biotechnol.*, vol. 21, pp. 1184–1191, Sep. 2003.
[38] B. Novák and J. J. Tyson, "Design principles of biochemical oscillators," *Nature Rev. Molecular Cell Biol.*, vol. 9, pp. 981–991, Dec. 2008.
[39] J. Stricker, S. Cookson, M. R. Bennett, W. H. Mather, L. S. Tsimring, and J. Hasty, "A fast, robust and tunable synthetic gene oscillator," *Nature*, vol. 456, nos. 516–519, Nov. 2008.
[40] J. T. Daub and R. M. H. Merks, "A cell-based model of extracellular-matrix-guided endothelial cell migration during angiogenesis," *Bull. Math. Biol.*, vol. 75, no. 8, pp. 1377–1399, 2013.
[41] D. G. Mallet and G. J. Pettet, "A mathematical model of integrin-mediated haptotactic cell migration," *Bull. Math. Biol.*, vol. 68, pp. 231–253, Feb. 2006.
[42] J. T. Smith, J. K. Tomfohr, M. C. Wells, T. P. Beebe, Jr., T. B. Kepler, and W. M. Reichert, "Measurement of cell migration on surface-bound fibronectin gradients," *Langmuir*, vol. 20, no. 19, pp. 8279–8286, 2004.
[43] J. T. Smith, J. T. Elkin, and W. M. Reichert, "Directed cell migration on fibronectin gradients: Effect of gradient slope," *Experim. Cell Res.*, vol. 312, no. 13, pp. 2424–2432, 2006.
[44] C.-H. Chan and Y.-H. Hsu, "A long range gradient-generating device for haptotaxis," in *Proc. 19th Nano Eng. Microsyst. Technol. Conf. (NMC)*, 2015, pp. 63–64.
[45] M. D. Abràmoff, P. J. Magalhães, and S. J. Ram, "Image processing with ImageJ," *Biophoton. Int.*, vol. 11, no. 7, pp. 36–42, 2004.
[46] E. Meijering, O. Dzyubachyk, and I. Smal, "Methods for cell and particle tracking," *Methods Enzymol.*, vol. 504, no. 9, pp. 183–200, 2012.
[47] S. Friberg and S. Mattson, "On the growth rates of human malignant tumors: Implications for medical decision making," *J. Surgical Oncol.*, vol. 65, no. 4, pp. 284–297, 1997.
[48] V. R. Muzykantov, "Targeted drug delivery to endothelial adhesion molecules," *ISRN Vascular Med.*, vol. 2013, Jun. 2013, Art. no. 916254.

Tadashi Nakano received the Ph.D. degree in information systems engineering from Osaka University, Japan, in 2002. He was with the Department of Computer Science, Donald Bren School of Information and Computer Sciences, University of California at Irvine, Irvine, CA, USA, where he was a Post-Doctoral Research Scholar from 2002 to 2007, and an Assistant Adjunct Professor from 2007 to 2009. From 2009 to 2013, he was an Associate Professor with the Graduate School of Engineering, Osaka University. He has been an Associate Adjunct Professor with the Institute of Academic Initiatives, Osaka University, since 2013, and a Visiting Associate Professor with the Graduate School of Biological Sciences. He is currently serving as the Chair of the IEEE Emerging Technical Subcommittee on Nano-scale, Molecular and Quantum Networking. He is also serving as an Associate Editor of the IEEE TRANSACTIONS ON MOLECULAR, BIOLOGICAL, AND MULTISCALE COMMUNICATIONS, an Associate Editor of the IEEE TRANSACTIONS ON NANOBIOSCIENCE, and an Editor of *Nano Communication Networks* (Elsevier). He has been engaged in research at the intersection of computer science and biology, including design, implementation, and evaluation of molecular communication systems, synthetic biological systems, and biologically inspired systems.

Yutaka Okaie received the B.Eng. degree from the Faculty of Engineering, Kobe University, Japan, in 2000, the M.Inf. degree from the Graduate School of Informatics, Kyoto University, Japan, in 2002, and the Ph.D. degree in information systems engineering from Osaka University, Osaka, Japan, in 2015. He was with the Department of Computer Science, Donald Bren School of Information and Computer Sciences, University of California at Irvine, Irvine, where he was a Research Assistant from 2006 to 2008. From 2009 to 2013, he was a Specially Appointed Researcher with the Frontier Research Center, Graduate School of Engineering, Osaka University. He has been a Specially Appointed Researcher with the Graduate School of Frontier Biosciences, Osaka University, since 2013. His current research interests include applied mathematics and modeling, and its applications to computer and communication systems.

Shouhei Kobayashi received the Ph.D. degree in engineering from Osaka University in 2005. He was with the Bio-ICT Group, National Institute of Information and Communications Technology (NICT) in 2005. He is currently a Planning Manager with NICT. His current research is focused on understanding cellular responses against invading artificial materials.

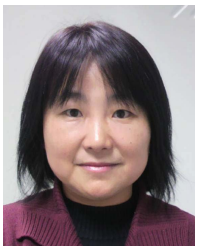

Takako Koujin received the B.A. degree in plant pathology from Kobe University, Kobe, Japan, in 1986. She has been a Laboratory Technician with the Bio-ICT Group, National Institute of Information and Communications Technology, since 1994.

Chen-Hao Chan received the B.S. degree in the Joint Science Program (majored in physics) from National Central University in 2014, the M.S. degree with the Institute of Applied Mechanics, National Taiwan University in 2016. His research interests include analytical analysis of the spin transport properties in spinfilter-based magnetic tunnel junction, collector designs for electrospinning process, and piezoelectric micro-platform for cardiac drug screening application.

Yu-Hsiang Hsu received the B.S. and M.S. degrees from the Department of Mechanical Engineering, Institute of Applied Mechanics, National Taiwan University, in 2000 and 2002, respectively, and the M.S. and Ph.D. degrees in biomedical engineering from the University of California at Irvine from 2006 to 2010. He was a Post-Doctoral Scholar with the California Institute of Technology and also with the University of California at Irvine. He has been with the Faculty of the Institute of Applied Mechanics, National Taiwan University, since 2013. His research primarily focuses on three fields: microsystems to develop microtissues for drug screening applications, including cardiac microtissue and microtumor, plastic lab-on-a-chip devices for early and quantitative diagnostic methods for chronic human diseases, and it can be integrated with portable devices, smart materials: develop optopiezoelectric composites for the applications of optically controllable pumps, valves, and sonic motors.

Takuya Obuchi is currently pursuing the master's degree in information systems engineering, Osaka University, Japan, where he is also a Student Researcher with the Department of Information and Communications Technology. His current research interests include interdisciplinary topics in the area of information networks, including molecular communication and nano-networks.

Takahiro Hara (M'98–SM'07) received the B.E., M.E., and Dr.Eng. degrees in information systems engineering from Osaka University, Osaka, Japan, in 1995, 1997, and 2000, respectively. Currently, he is a Professor with the Department of Multimedia Engineering, Osaka University. His research interests include distributed databases, mobile computing, and social computing. He has authored over 400 international journal and conference papers. He served as a Program Chair of IEEE MDM'06 and 10, IEEE AINA'09 and 14, IEEE SRDS'12, Mobiquitous'13, IEEE UIC'14, and DaWaK'15 and 16. He is a Distinguished Scientist of ACM, and a member of three other learned societies.

Yasushi Hiraoka received the Ph.D. degree in biophysics from Kyoto University in 1985. He was with the University of California at San Francisco, San Francisco, CA, USA, from 1985 to 1991, and with the National Institute of Information and Communications Technology from 1991 to 2007. Currently, he is a Professor with Osaka University. His current research aims to understand structures and functions of the cell nucleus.

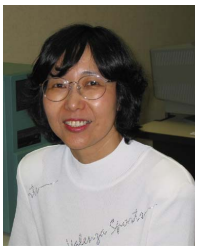

Tokuko Haraguchi received the bachelor's and master's degrees from Ochanomizu University in 1977 and 1979, respectively, and the Ph.D. degree from the School of Medicine, University of Tokyo, in 1985. She was with the University of California from 1985 to 1991, and the Bio-ICT Group, National Institute of Information and Communications Technology (NICT), Japan, from 1992 to 2016. Currently, she is a Senior Researcher with NICT. She has been a Professor with the Graduate School of Science, Osaka University, since 1997, where she has been a Professor with the Graduate School of Frontier Biosciences, since 2008. Her current research is focused on understanding of cellular functions by developing imaging technology to visualize molecular dynamics in living cells.